

Electron transport in multiterminal molecular devices: A density functional theory studyKamal K. Saha,¹ Wenchang Lu,^{1,2} J. Bernholc,^{1,2} and Vincent Meunier^{1,3,*}¹Computer Science and Mathematics Division, Oak Ridge National Laboratory, Oak Ridge, Tennessee 37831-6367, USA²Center for High Performance Simulation and Department of Physics, North Carolina State University, Raleigh, North Carolina 27695-7518, USA³Center for Nanophase Materials Science, Oak Ridge National Laboratory, Oak Ridge, Tennessee 37831-6367, USA

(Received 4 August 2009; revised manuscript received 15 February 2010; published 18 March 2010)

The electron transport properties of a four-terminal molecular device are computed within the framework of density functional theory and nonequilibrium Keldysh theory. The additional two terminals lead to new properties, including a pronounced negative differential resistance not present in a two-terminal setup, and a pseudogating effect. In general, quantum interference between the four terminals and the central molecule leads to a complex nonlinear behavior of the current, which depends on the alignment of individual molecular states under bias and their coupling to the leads.

DOI: [10.1103/PhysRevB.81.125420](https://doi.org/10.1103/PhysRevB.81.125420)

PACS number(s): 85.65.+h, 72.10.-d, 73.63.-b, 85.35.-p

I. INTRODUCTION

In recent years, numerous papers have been published to investigate the connection between the microscopic characteristics of an electronic system, such as atomic configuration and electronic structure, and the electron transport properties, such as electrical current and conductance.¹⁻⁸ These results have substantially improved the general understanding of the *I-V* characteristic of nanojunctions. While it is still difficult to fully determine the atomic geometries of measured junctions and to establish a one-to-one correspondence between the observed and the calculated results,⁹ there has been significant progress in both experimental and theoretical capabilities. For example, recent findings further highlight transport mechanisms driven by individual molecular orbitals in a two-terminal setup transport.^{10,11} As the interest increasingly focuses on more complicated nanoelectronic devices, several groups have theoretically addressed aspects of electron transport in multiterminal geometries,¹²⁻¹⁶ but they did not include an *ab initio* treatment of electron transport and lacked a self-consistent charge-density adjustment with the increase of the bias. In fact, all of the existing *ab initio* approaches to electron transport that we are aware of have dealt only with two-terminal systems.^{3,4,17-21} It is however of general interest to develop robust computational schemes that can routinely and reliably account for the transport mechanism in multiterminal molecular junctions, as these are critically important in both fundamental studies and applications. Even in classical measurements of key electrical properties, four-terminal techniques are vastly more accurate and reliable than the two-terminal ones. Although such measurements are very difficult in nanoscale systems, four-probe scanning tunneling microscopy (STM) enables a rather complete characterization of electron conductance in potential building blocks for molecular and nanoscale electronics.²² Furthermore, multiterminal structures are critical for applications. For instance, it is impossible to achieve amplification using only two terminal structures.²³ This is because all electronic circuits have some loss and therefore require multistage amplification. While simple logic operations could in principle be performed without amplification, modern computing operations consist of many such steps, which inevitably result in

the need for amplification. This need is even greater in sensors and antennas, which must greatly amplify very weak signals to ensure detection and communication. Despite the importance of multiterminal devices, multiterminal aspects at the nanoscale level have hardly been investigated either experimentally or theoretically, except in the “field-effect-transistor” geometry, in which a gating potential is applied through a well-insulated macroscopic gate without any possibility of leakage current through the gate electrode.²³⁻²⁸ While this geometry is very useful in classical devices, the effects of leakage in molecular-scale devices with a nanoscale gate electrode can be substantial. In addition, quantum effects are exacerbated at this scale, potentially resulting in novel and unforeseen phenomena.

In this paper we describe the results of a state-of-the-art *ab initio* study of a four-terminal device consisting of an organic molecule connected to four gold nanowires. We use a recently developed multiterminal formalism²⁹ and employ self-consistent density functional theory in the context of a nonequilibrium Green’s function method.^{30,31} We find that the presence of additional terminals leads to new effects, including unexpected quantum interference patterns that can be explored in practical devices and, more notably, the emergence of a strong negative differential resistance (NDR), which is otherwise not present in the corresponding two-terminal device.

The molecular system investigated here is represented in the inset of Fig. 1. It consists of a [9, 10-Bis((2'-para-mercaptophenyl)-ethynyl)-anthracene] molecule connected via thiol bridges to four gold nanowires. While this system is challenging to realize experimentally with current nanomanipulation techniques, similar geometries can be achieved using a four-probe STM for molecules deposited on an insulating substrate. In a two-terminal geometry, two main factors govern the *I-V* characteristics: the position and properties of orbitals originating from the free molecule (we call them pseudomolecular orbitals), and details of the contacts between the molecule and the electrodes. While these factors are also important in multiterminal setups, the intricacies of mutual couplings between the individual probes give rise to even more complex *I-V* characteristics. The molecule shown in Fig. 1 has already been

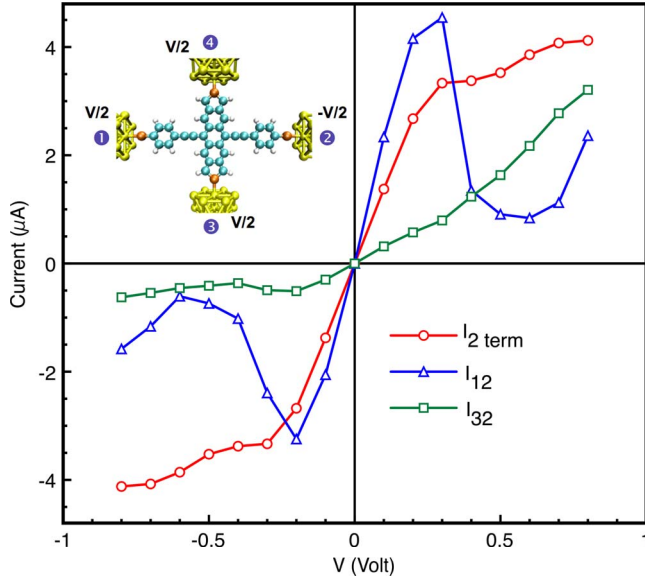


FIG. 1. (Color online) I - V curves of the four-terminal molecular device. For comparison, the I - V curve (I_2) of the corresponding two-terminal 1–2 setup is also shown. In the inset, the bias geometry of the four-terminal system is schematically displayed. Au, S, C, and H atoms are shown in yellow (in the lead region), red (black), cyan (large gray), and gray (small gray), respectively. The semi-infinite leads are built out of Au(111) nanowires.

investigated in a two-terminal configuration. Reichert *et al.*³² reported an experimental investigation of this and a related molecule in a break junction geometry. While the precise atomic structures of the contacts were not determined, the authors presented strong arguments that they have measured single molecule I - V characteristics. Heurich *et al.*³³ performed DFT-tight-binding calculations for the same system, obtaining results in qualitative agreement with experiment. In both experiment and theory, the I - V curves are smooth and symmetric about the zero voltage line, with no negative differential resistance (NDR) effects.

II. METHODOLOGY AND CALCULATIONS

The present calculations are carried out using a recently developed multiterminal formalism that allows for self-consistent DFT calculations of I - V characteristics of complex nanojunctions.²⁹ All quantities are computed at the density functional theory (DFT) level with full self-consistency (SC) under applied bias, using ultrasoft pseudopotentials³⁴ and Perdew-Burke-Ernzerhof exchange-correlation functional.³⁵ We follow a four-step approach: first, sets of atom-centered localized orbitals are variationally optimized for the leads and the central molecule.³⁶ We use 10, 6, and 4 orbitals per Au, C, and H atoms, respectively, all with a radius of 4.3 Å. Each of the four electrodes is simulated by an Au(111) nanowire^{37–39} built from (111) subunits. The periodic subunit is made up of three layers containing 7, 6, and 6 atoms, respectively. Several other nanowire configurations were considered and our careful checks of the layer size indicate that this model wire yields a realistic representation of gold

nanoscale electrodes, e.g., by having the same number of conducting channels to the molecule as a bulk Au lead around the Fermi energy. The extended scattering region S includes the molecule and 8 layers of Au in each lead. The inclusion of the 8 “extended buffer” layers ensures a proper treatment of the molecule-lead coupling,⁴⁰ as well as proper screening of the potential drop in the leads. (When a single chain of Au atoms is used as an electrode, the screening length is much longer than in bulk Au or the Au nanowire employed above, and the 8 “extended buffer” layers are no longer able to eliminate an artificial potential drop at the interface.) Second, the conductor’s Green’s function, coupling matrices and self-energies are expanded within this basis set, and the charge density and potentials are calculated self-consistently for the combined system at zero bias. During the self-consistency process, the Hartree potential is obtained by solving Poisson equation in the S region with boundary conditions that match the electrostatic potential of all the leads. Third, after the charge density for the combined system is converged at zero bias, a realistic bias potential is applied.^{29,41} The nonequilibrium Green’s function (NEGF), charge density, and potentials of the four-terminal junction are computed through a self-consistent process²⁹ using Keldysh formalism.^{21,41} Finally, the current from the lead i through the molecular barrier to lead j , driven by the bias $V(eV = \mu_i - \mu_j)$, is obtained from

$$I_{ij}(V) = \frac{2e}{h} \int_{-\infty}^{\infty} T_{ij}(\varepsilon, V) [f(\varepsilon - \mu_i) - f(\varepsilon - \mu_j)] d\varepsilon, \quad (1)$$

where f is the Fermi function and T_{ij} is the energy- and voltage-dependent transmission spectrum from the i th to j th lead, which also self-consistently depends on the voltages applied to the other leads through the Hartree potential acting on the electrons.

III. RESULTS AND DISCUSSION

In the DFT-optimized geometry presented in Fig. 1, two ends of the molecule are covalently connected to Au leads via thiol bridges. The other two ends are connected to Au leads via thiophene groups.⁴² For a two-terminal setup without leads 3 and 4, our calculated I - V curve (I_2 term curve in Fig. 1) shows no NDR features, in agreement with experiment. The absolute value of the current is substantially larger than the experimental one.³² Apart from the likely difference in contact geometries between our calculations and the experiment, it is well known that DFT underestimates the HOMO-LUMO gap, which also results in an overestimation of the current.⁴³ Our current is also larger than that computed previously.³³ In the previously reported study, a single Au atom was used to connect the molecule to the Au electrode, and the electrode-molecule coupling was determined by a tight-binding parameter. In fact, the reduced number of conduction channels alone can largely account for the difference with our DFT-based calculation using more realistic leads.

A. Pronounced negative differential resistance

In a four-terminal junction, many distributions of bias voltages are possible. In the following, we will consider two

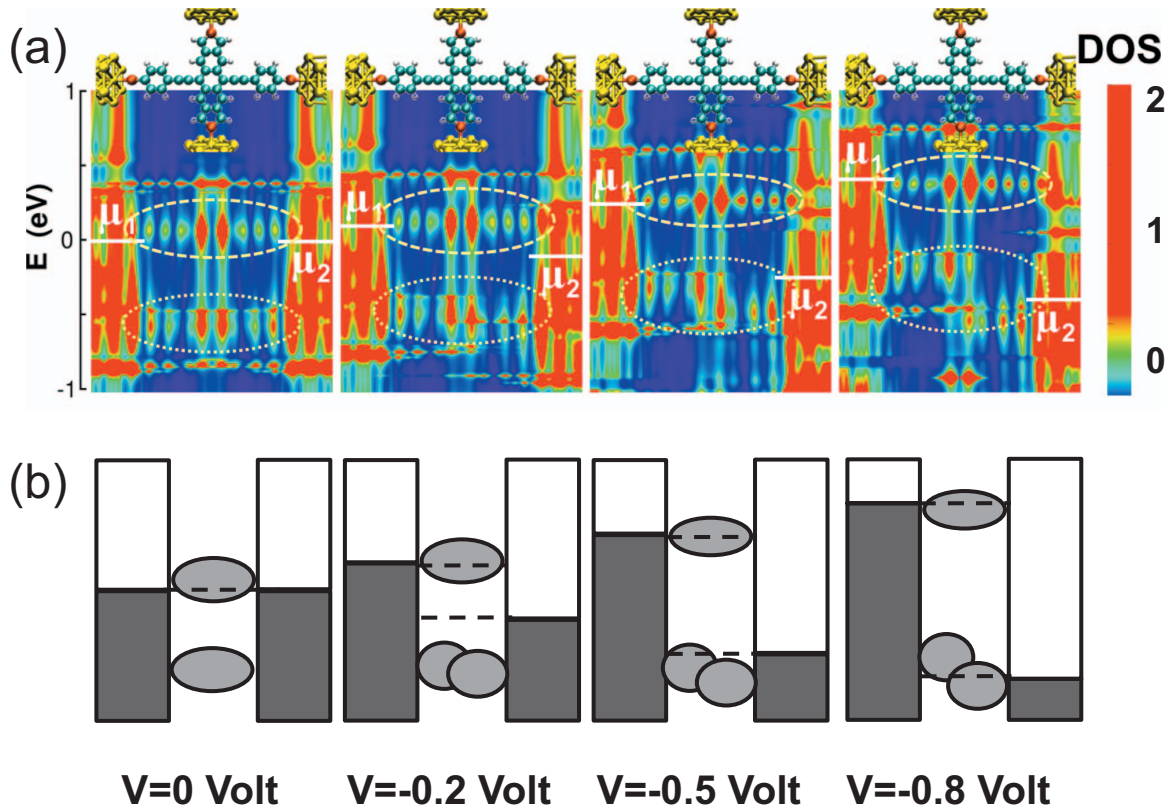


FIG. 2. (Color) (a) Position-dependent density of states along the left-to-right direction at biases of 0.0, -0.2 , -0.5 , and -0.8 V. The DOS is averaged in the plane perpendicular to the current. Note that the electronic states originating from the vertical leads are not included in the figure. The chemical potentials of the left and right leads are shown as white lines. The zero of energy is at $(\mu_1 + \mu_2)/2$. The dotted and dashed ovals enclose the pseudomolecular states that originate from the highest occupied and lowest unoccupied molecular orbitals, respectively. To make it clearer, the bottom panel (b) illustrates only the main features of the DOS, and the alignment and broadening of the LUMO and HOMO states.

special cases. In the first one, an identical bias potential $V/2$ is applied to leads 1, 3, and 4, while $-V/2$ is applied to lead 2 (see the inset in Fig. 1). Using this bias distribution, we find that the I_{12} current (Fig. 1) is asymmetric and presents a pronounced NDR. This finding is in striking contrast with the two-terminal result, where the I - V characteristic is much smoother, with no NDR. In this four-terminal geometry the I_{32} current (Fig. 1) is very different from I_{12} , showing pronounced asymmetry between the forward and reverse directions, as well as a weak NDR around $V = -0.2$ V.

The shapes of the different I - V curves in the four-terminal geometry can be explained by analyzing the behavior of individual pseudomolecular states under bias and the relative strength of their coupling with the four electrodes. The position-dependent density of states (DOS) can be calculated by⁴¹

$$\rho(r, E) = \frac{1}{\pi} \sum_{i,j} \Phi_i^*(r) \text{Im}[G_{ij}(E)] \Phi_j(r),$$

where $\phi_i(r)$ are the optimized orbitals and $G_{ij}(E)$ the Green's functions of the system. Figure 2(a) shows the DOS averaged over y and z directions (x direction is along the left-to-right electrodes). The zero of energy is chosen to be the average of the chemical potentials of lead 1 and lead 2,

$(\mu_1 + \mu_2)/2$. The LUMO state, located at 74 meV (dashed-oval) at the equilibrium (no bias applied), follows rigidly the changes in μ_1 and extends all the way from the left to the right electrode. The plot of the computed local density of states contains a wealth of data that can be confusing. In

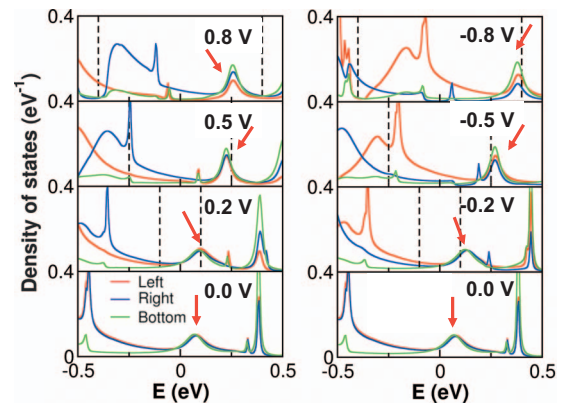


FIG. 3. (Color) Changes in the pseudomolecular states with the bias voltage. The densities of states close to the left, right, and bottom molecule-lead interfaces (of leads 1, 2, and 3) are shown. Due to the symmetry in the bias geometry, the electronic structures at the top and bottom interfaces are identical. The red arrow indicates the position of the LUMO, which mainly drives the current.

order to facilitate interpretation we also provide a simplified representation of this information in Fig. 2(b). The HOMO state, located at -0.44 eV (dotted-oval) at the equilibrium, is spatially split between the left and right electrodes, each end being pinned to major features of its respective lead. The HOMO and LUMO states are individual energy levels in an isolated molecule. When the molecule is connected to the electrodes, these states are modified in two ways. First, they broaden due to coupling between the molecule and the electrodes. The broadening of the HOMO and LUMO states reflects the strength of the coupling and the finite lifetime of an electron on that state (hence leading to improved conduction). Second, the coupling leads to level shifts relative to the Fermi level. When bias is applied, parts of the broadened LUMO enter the bias window in such a way that the LUMO contributes the most of the total current. Comparing the LUMO state at bias -0.5 V with that at bias -0.2 V, one can clearly see that the LUMO state is less broadened at bias -0.5 V, indicating that the coupling between the molecule and the electrode becomes weaker. As a result, the current (the curve I_{12} in Fig. 1) decreases when the bias decreases from -0.2 to -0.5 V, and an NDR feature appears. This situation occurs for both positive and negative biases.

To examine the coupling in detail, we plot in Fig. 3 the local densities of states near the lead-molecule interfaces for various bias potentials. For the left or the right lead-molecule interface, the DOS (red or blue curves in Fig. 3) are localized at the sulfur and its nearby benzene ring. For the bottom lead-molecule interface, the DOS (green curve in Fig. 3) are localized at the sulfur and its nearby six carbon atoms. The left-to-right I - V curve (I_{12} in Fig. 1) can be understood by monitoring the position of the LUMO (red arrows). As the bias increases from 0.0 to 0.8 V, the width of the LUMO slowly increases until 0.2 V, resulting in an essentially linear increase in the current with an increase in the bias window (marked by dotted vertical lines in Fig. 3.). At 0.5 V, the coupling with the electrodes suddenly decreases due to the action of the potential applied to the three electrodes at positive bias, which results in a nonlinear I - V curve. In fact, in the two-terminal geometry, the coupling at 0.5 V is also weaker than the coupling at 0.2 V. This results in flattening of the red curve in Fig. 1, but it is not large enough to lead to an NDR. As the bias increases further, the current grows again. This is due to the increasing bias window and strengthening of the coupling. A similar explanation holds for the negative bias, with slight variations in the positions and spreads of HOMO and LUMO within the bias window, which account for the changes in current amplitudes. In addition, we note some differences between positive (left panel in Fig. 3) and negative (right panel in Fig. 3) biases. At biases smaller than 0.5 V in absolute value, the center of the LUMO state is outside the bias window for negative bias, but is inside the bias window for positive bias. This results in a larger current at positive bias than at negative bias. Turning to the bottom-to-right (I_{32}) or top-to-right (I_{42}) currents, which are equal by symmetry, the current amplitudes for the negative bias are substantially smaller than those for the positive bias. The negative bias induces a possible current-carrying state at the top, bottom, and left sides, but without a corresponding level at the right collecting electrode. There-

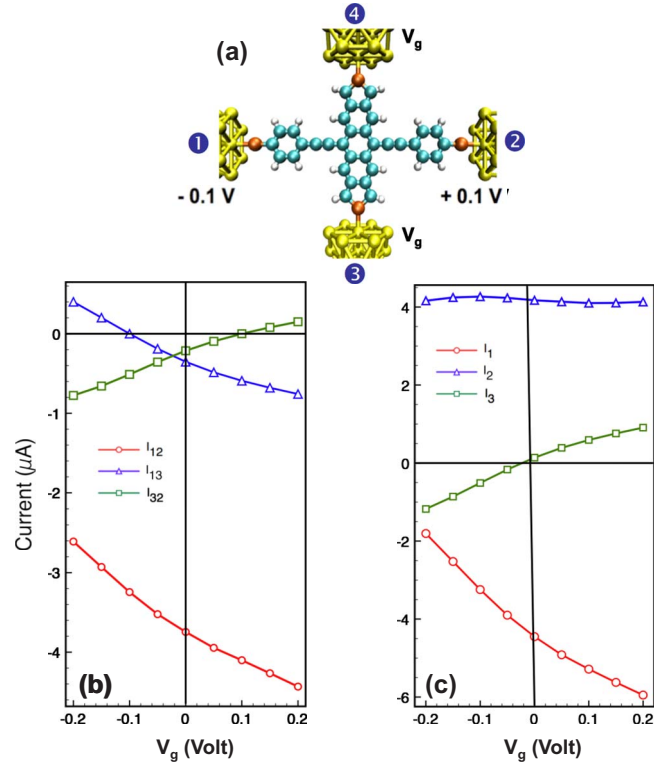


FIG. 4. (Color online) Currents in the four-terminal geometry shown in (a) as a function of pseudogate voltage V_g . (b) Currents I_{ij} passing through terminals i and j . A positive (negative) I_{ij} indicates electrons flow from electrode i (j) to electrode j (i). (c) Total currents I_i passing through terminals i . The currents I_3 and I_4 are equal by symmetry. $I_i > 0$ indicates electrons entering electrode i and $I_i < 0$ indicates electrons leaving electrode i .

fore, the current remains small. The situation is different for positive bias, where a current-carrying level exists at the top, bottom, and right electrodes. This level is quite broad, indicating good coupling and thus a large current. The apparent asymmetry in the positive and negative biases is thus due to the specific bias configuration we applied.

B. Pseudogate effect

As stated above, various combinations of bias distributions are possible. In the second distribution examined in this paper, we focus on a configuration that mimics the presence of a pseudo-gate voltage V_g , applied to the top (terminal 4) and bottom (terminal 3) electrodes, shown in Fig. 4(a). The voltages on terminals 1 and 2 are fixed at -0.1 and $+0.1$ V respectively. The pseudogate voltage is swept from -0.2 to 0.2 V [Fig. 4(a)]. This is not a typical gate (hence the adjective “pseudo”), because the pseudogate is not separated from the source-drain channel by an insulating layer and a quite large leakage current is expected, in light of the results shown above. The currents I_{ij} , flowing from terminal i to j , are calculated by Eq. (1) and shown in Fig. 4(b). As the pseudogate voltage V_g increases, the source-to-drain current I_{12} decreases. At equilibrium (no applied bias in any terminal), the LUMO state of the central molecule is just above the Fermi level of the leads. Figure 5 shows a representation

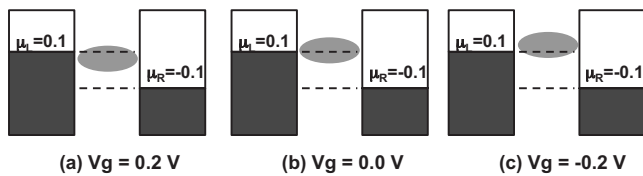


FIG. 5. Illustration of LUMO shift under different pseudogate voltages. The largest part of the broadened LUMO state (shaded oval) is in the bias window for positive pseudogate voltages. When the pseudogate voltage is negative, the LUMO state moves up and only a small part of the broadened LUMO is in the bias window.

of the relative alignment of the LUMO state under different pseudogate voltage V_g . The LUMO state is shifted down for positive V_g and mostly falls into the bias window, thereby yielding a large absolute current. When V_g is negative, the LUMO state is shifted up. As a result, the LUMO state moves away from the bias window. Therefore, the absolute value of the current I_{12} increases when the pseudogate voltage sweeps from -0.2 to 0.2 V. The absolute value of the source-to-gate current I_{13} at positive pseudogate voltage is also larger than that at negative pseudogate voltage. This is due to two factors. The first one is the same as that explained above for the variation of I_{12} . The second reason is that the bias window for the source-gate current expands as V_g increases from -0.2 to 0.2 V. However, the gate-to-drain current I_{32} has the opposite behavior. This is mainly due to the large bias window for the gate-drain current at negative V_g . Figure 4(b) also shows that the leakage currents I_{32} and I_{31} are much smaller in absolute values than the source-to-drain

current I_{12} . By symmetry, I_{41} and I_{42} are identical to I_{31} and I_{32} .

IV. SUMMARY

In summary, we have presented a DFT study of a four-terminal molecular system, highlighting features that are absent in conventional two-terminal setups. The results show counterintuitive features induced by the quantum-mechanical interplay between the four terminals, including the introduction of a large negative differential resistance that is absent in a two-terminal geometry. The currents between the different terminals are dissimilar and highly nonlinear, due to the complex effect of a spatially intricate bias potential interacting with electronic levels of the central region. While the flexibility of a multiterminal device and its varying responses to biases applied at different terminals remain to be explored and categorized, they open the possibility of novel, multifunctional device structures with nanoscale dimensions.

ACKNOWLEDGMENTS

This research was sponsored in part by the Laboratory Directed Research and Development Program of Oak Ridge National Laboratory (ORNL), managed by UT-Battelle, LLC for the U. S. Department of Energy under Contract No. DE-AC05-00OR22725. Work at NCSU was partially funded by DOE Grant No. DE-FG02-98ER45685 and ONR Grant No. N000141010179.

*Corresponding author; meunierv@ornl.gov

- ¹A. Nitzan and M. A. Ratner, *Science* **300**, 1384 (2003).
- ²M. A. Reed, C. Zhou, C. J. Muller, T. P. Burgin, and J. M. Tour, *Science* **278**, 252 (1997).
- ³K. H. Bevan, D. Kienle, H. Guo, and S. Datta, *Phys. Rev. B* **78**, 035303 (2008).
- ⁴M. Galperin, M. A. Ratner, and A. Nitzan, *Nano Lett.* **9**, 758 (2009).
- ⁵A. Danilov, S. Kubatkin, S. Kafanov, P. Hedegard, N. Stuhr-Hansen, K. Moth-Poulsen, and T. Bjornholm, *Nano Lett.* **8**, 1 (2008).
- ⁶T. Rakshit, G. C. Liang, A. W. Ghosh, and S. Datta, *Nano Lett.* **4**, 1803 (2004).
- ⁷Y. Xue, S. Datta, S. Hong, R. Reifengerger, J. I. Henderson, and C. P. Kubiak, *Phys. Rev. B* **59**, R7852 (1999).
- ⁸A. W. Ghosh and S. Datta, *J. Comput. Electron.* **1**, 515 (2002).
- ⁹S. M. Lindsay and M. A. Ratner, *Adv. Mater.* **19**, 23 (2007).
- ¹⁰J. Kushmerick, *Nature (London)* **462**, 994 (2009).
- ¹¹H. Song, Y. Kim, Y. H. Jang, H. Jeong, M. A. Reed, and T. Lee, *Nature (London)* **462**, 1039 (2009).
- ¹²M. Büttiker, *Phys. Rev. Lett.* **57**, 1761 (1986).
- ¹³H. U. Baranger, D. P. DiVincenzo, R. A. Jalabert, and A. D. Stone, *Phys. Rev. B* **44**, 10637 (1991).
- ¹⁴S. Ami and C. Joachim, *Phys. Rev. B* **65**, 155419 (2002).
- ¹⁵A. Pecchia, G. Penazzi, L. Salvucci, and A. Di Carlo, *New J. Phys.* **10**, 065022 (2008).
- ¹⁶K. Kazymyrenko and X. Waintal, *Phys. Rev. B* **77**, 115119 (2008).
- ¹⁷S.-H. Ke, H. U. Baranger, and W. Yang, *Phys. Rev. B* **71**, 113401 (2005).
- ¹⁸M. Koentopp, C. Chang, K. Burke, and R. Car, *J. Phys.: Condens. Matter* **20**, 083203 (2008).
- ¹⁹R. Li, J. X. Zhang, S. M. Hou, Z. K. Qian, Z. Y. Shen, X. Y. Zhao, and Z. Q. Xue, *Chem. Phys.* **336**, 127 (2007).
- ²⁰K. Stokbro, *J. Phys.: Condens. Matter* **20**, 064216 (2008).
- ²¹M. Brandbyge, J.-L. Mozos, P. Ordejón, J. Taylor, and K. Stokbro, *Phys. Rev. B* **65**, 165401 (2002).
- ²²I. Shiraki, F. Tanabe, R. Hobara, T. Nagao, and S. Hasegawa, *Surf. Sci.* **493**, 633 (2001).
- ²³R. Waser, *Nanoelectronics and Information Technology* (Wiley-VCH, New York, 2005).
- ²⁴S. Kubatkin, A. Danilov, M. Hjort, J. Cornil, J. L. Bredas, N. Stuhr-Hansen, P. Hedegard, and T. Bjornholm, *Nature (London)* **425**, 698 (2003).
- ²⁵C. R. Kagan, D. B. Mitzi, and C. D. Dimitrakopoulos, *Science* **286**, 945 (1999).
- ²⁶S. S. Datta, D. R. Strachan, and A. T. C. Johnson, *Phys. Rev. B* **79**, 205404 (2009).
- ²⁷C. A. Stafford, D. M. Cardamone, and S. Mazumdar, *Nanotechnology* **18**, 424014 (2007).

- ²⁸D. L. Klein, R. Roth, A. K. L. Lim, A. P. Alivisatos, and P. L. McEuen, *Nature (London)* **389**, 699 (1997).
- ²⁹K. K. Saha, W. C. Lu, J. Bernholc, and V. Meunier, *J. Chem. Phys.* **131**, 164105 (2009).
- ³⁰R. Haug and A.-P. Jauho, *Quantum Kinetics in Transport, Optics of Semiconductors* (Springer-Verlag, Berlin, 1996).
- ³¹S. Datta, in *Electronic Transport in Mesoscopic Systems*, edited by H. Ahmed, M. Pepper, and A. Broers (Cambridge University Press, Cambridge, England, 1995).
- ³²J. Reichert, R. Ochs, D. Beckmann, H. B. Weber, M. Mayor, and H. v. Löhneysen, *Phys. Rev. Lett.* **88**, 176804 (2002).
- ³³J. Heurich, J. C. Cuevas, W. Wenzel, and G. Schön, *Phys. Rev. Lett.* **88**, 256803 (2002).
- ³⁴D. Vanderbilt, *Phys. Rev. B* **41**, 7892 (1990).
- ³⁵J. P. Perdew, K. Burke, and M. Ernzerhof, *Phys. Rev. Lett.* **77**, 3865 (1996).
- ³⁶J. L. Fattebert and J. Bernholc, *Phys. Rev. B* **62**, 1713 (2000).
- ³⁷H. Kondo, H. Kino, J. Nara, T. Ozaki, and T. Ohno, *Phys. Rev. B* **73**, 235323 (2006).
- ³⁸S.-H. Ke, H. U. Baranger, and W. Yang, *Phys. Rev. B* **70**, 085410 (2004).
- ³⁹C. Zhang, Y. He, H. P. Cheng, Y. Q. Xue, M. A. Ratner, X. G. Zhang, and P. Krstic, *Phys. Rev. B* **73**, 125445 (2006).
- ⁴⁰M. B. Nardelli, J. L. Fattebert, and J. Bernholc, *Phys. Rev. B* **64**, 245423 (2001).
- ⁴¹W. C. Lu, V. Meunier, and J. Bernholc, *Phys. Rev. Lett.* **95**, 206805 (2005).
- ⁴²H. H. Cho, H. Y. Chang, E. H. Kim, Y. C. Park, and Z. U. Bae, *Bull. Korean Chem. Soc.* **27**, 1701 (2006).
- ⁴³M. Di Ventra, S. T. Pantelides, and N. D. Lang, *Phys. Rev. Lett.* **84**, 979 (2000).